Inorg. Chem. **2004**, *43*, 3394–3405

Dynamic Structural Change of a Twisted Hexaporphyrin Complex by Highly Specific Molecular Recognition

Hiroaki Kitagishi, Akiharu Satake, and Yoshiaki Kobuke*

Graduate School of Materials Science, Nara Institute of Science and Technology, 8916-5 Takayama, Ikoma, Nara 630-0192, Japan

Received March 17, 2004

The highly specific molecular recognition of a twisted hexaporphyrin complex, tris[5,5′-bis[5,10,15-tris{methoxy-(ethoxy)$_2$carbonylethyl}porphyrinatozinc(II)]-2,2′-bipyridine]ruthenium(II) chloride (**2**), is described. Complex **2** has two trisporphyrin binding sites and can bind two triamines, tris(2-aminoethyl)amine (**3**) ($K_1 = 3.0 \times 10^8$ M^{-1}, $K_2 = 3.0 \times 10^7$ M^{-1}), 1,1,1-tris(aminomethyl)ethane (**4**) ($K_1 = 2.0 \times 10^7$ M^{-1}, $K_2 = 1.4 \times 10^6$ M^{-1}), tris(3-aminopropyl)-amine (**5**) ($K_1 = 3.5 \times 10^6$ M^{-1}, $K_2 = 6.0 \times 10^6$ M^{-1}), and 1,3,5-tris(aminomethyl)benzene (**6**) ($K_1 = 2.9 \times 10^6$ M^{-1}, $K_2 = 1.2 \times 10^6$ M^{-1}), strongly with its torsional motion. The 1:2 complex between **2** and the best fit triamine **3** showed the nature of the specific rigid structure in the UV–vis, fluorescence, and ^{1}H NMR spectra and isothermal titration calorimetry (ITC) measurements.

Introduction

Multiple-porphyrin systems of well-regulated structures are of great interest as molecular devices for photo/electronic applications.[1] Various types of multiporphyrins have been reported as mimics of light harvesting antenna complexes,[1d,e,2] nonlinear optical devices,[3] and cooperative binding hosts.[4] Their properties depend on three-dimensional geometry, linking units, and dynamic properties as well as the individual characteristics of the porphyrin unit. Therefore, the precise arrangement of the geometry of the porphyrins in such assemblies is important to improve such devices. Fixation of a multiporphyrin system in a certain rigid structure is also important to maintain the desired structure so that energy and electron transfer may proceed smoothly without deactivation processes through various energy states finally to the sink. We have examined a way to construct multiporphyrin systems by self-assembly.[5] To develop such systems, coordinative heteroaromatic ligands were attached directly to porphyrin rings. Coordination of the directly connected ligand afforded rigid multiporphyrin supramolecules. Imidazolylporphyrin derivatives gave rigid dimers,[6] straight oligomers, giant wires,[7] and macrocyclic rings[2b,c] by self-assembled complementary coordination. On the other hand, when bidentate ligands, such as oxine[8] and 2,2′-bipyridine,[9] were directly attached to the porphyrin ring, spatial positions were controlled by the outer metal ion. In the latter case,

* Author to whom correspondence should be addressed. Fax: (+81)-743-72-6119. Phone: (+81)743-72-6110. E-mail: kobuke@ms.naist.jp.

(1) Reviews: (a) Chambron, J.-C.; Heitz, V.; Sauvage, J.-P. In *The Porphyrin Handbook*; Kadish, K. M., Smith, K. M., Guilard, R., Eds.; Academic Press: New York, 2000; Vol. 6, pp 1−42. (b) Sanders, J. K. M. In *The Porphyrin Handbook*; Kadish, K. M., Smith, K. M., Guilard, R., Eds.; Academic Press: New York, 2000; Vol. 3, pp 347−368. (d) Aratani, N.; Osuka, A. *Bull. Chem. Soc. Jpn.* **2001**, *74*, 1361−1379. (e) Holten, D.; Bocian, D. F.; Lindsey, J. S. *Acc. Chem. Res.* **2002**, *35*, 57−69.

(2) (a) Choi, M.-S.; Aida, T.; Yamazaki, T.; Yamazaki, I. *Chem.*−*Eur. J.* **2002**, *8*, 2667−2678. (b) Takahashi, R.; Kobuke, Y. *J. Am. Chem. Soc.* **2003**, *125*, 2372−2373. (c) Ikeda, C.; Satake, A.; Kobuke, Y. *Org. Lett.* **2003**, *5*, 4935−4938.

(3) (a) Ogawa, K.; Zhang, T.; Yoshihara, K.; Kobuke, Y. *J. Am. Chem. Soc.* **2002**, *124*, 22−23. (b) Ogawa, K.; Ohashi, A.; Kobuke, Y.; Kamada, K.; Ohta, K. *J. Am. Chem. Soc.* **2003**, *125*, 13356−13357. (c) Kuebler, S. M.; Denning, R. G.; Anderson. H. L. *J. Am. Chem. Soc.* **2000**, *122*, 339−347. (d) Screen, T. E. O.; Thorne, J. R. G.; Denning, R. G.; Bucknall, D. G.; Anderson, H. L. *J. Am. Chem. Soc.* **2002**, *124*, 9712−9713.

(4) Review: (a) Sanders, J. K. M. In *Comprehensive Supramolecular Chemistry*; Atwood, J. L., Davies, J. E. D., MacNicol, D. D., Vogtle, F., Eds.; Pergamon Press: Oxford, 1996; Vol. 9, pp 131−164. Recent reports: (b) Kurtan, T.; Nesnas, N.; Li, Y.-Q.; Huang, X.; Nakanishi, K.; Berova, N. *J. Am. Chem. Soc.* **2001**, *123*, 5962−5973. (c) Kurtan, T.; Nesnas, N.; Koehn, F. E.; Li, Y.-Q.; Nakanishi, K.; Berova, N. *J. Am. Chem. Soc.* **2001**, *123*, 5974−5982. (d) Tashiro, K.; Aida, T.; Zheng, J.-Y.; Kinbara, K.; Saigo, K.; Sakamoto, S.; Yamaguchi, K. *J. Am. Chem. Soc.* **1999**, *121*, 9477−9478. (e) Borovkov, V. V.; Lintuluoto, J. M.; Sugeta, H.; Fujiki, M.; Arakawa, R.; Inoue, Y. *J. Am. Chem. Soc.* **2002**, *124*, 2993−3006. (f) Kubo, Y.; Ohno, T.; Yamanaka, J.-i.; Tokita, S.; Iida, T.; Ishimaru, Y. *J. Am. Chem. Soc.* **2001**, *123*, 12700−12701. (g) Sirish, M.; Schneider, H.-J. *J. Am. Chem. Soc.* **2000**, *122*, 5881−5882.

(5) Kobuke, Y.; Ogawa, K. *Bull. Chem. Soc. Jpn.* **2003**, *76*, 689−708.

(6) Kobuke, Y.; Miyaji, H. *J. Am. Chem. Soc.* **1994**, *116*, 4111−4112.

(7) (a) Ogawa, K.; Kobuke, Y. *Angew. Chem., Int. Ed.* **2000**, *39*, 4070−4073. (b) Ikeda, C.; Fujiwara, E.; Satake, A.; Kobuke, Y. *Chem. Commun.* **2003**, 616−617.

10.1021/ic049645g CCC: $27.50
Published on Web 05/01/2004

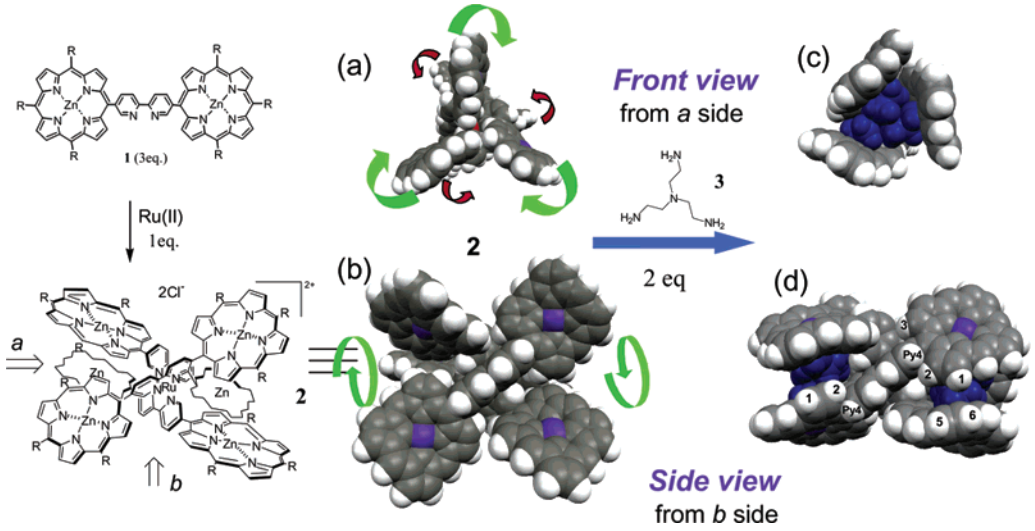

Figure 1. Space-filling pictures of the molecular structure: (a) front view of **2** before complexation, (b) side view of **2**, (c) front view of the **2**/amine **3** complex, and (d) side view of the **2**/amine **3** complex. Alkyl chains in meso positions are eliminated for clarity.

central metals in the porphyrins are employed further for coordination with outer ligands. These multiporphyrin systems are expected to exhibit characteristic properties which could not be observed in single-porphyrin systems. One of our targets of self-assembled multiporphyrins has been the trisbipyridine metal complex {M(bipy)$_3$} type hexaporphyrin **2**, which is very attractive for reasons described in the Design and Molecular Modeling section. Here, we report an efficient synthesis of complex **2** and its specific binding with triamine ligands accompanied by dynamic structural change.

Design and Molecular Modeling

Hexaporphyrin **2** may be easily constructed from bipyridine bisporphyrin **1** with the use of a hexacoordinating metal ion and is expected to be an intelligent multiporphyrin complex for the following reasons: (1) Six porphyrins locate within only a ca. 2 nm sphere, and effective excited energy delocalization is expected. (2) Strong electronic coupling among porphyrins is expected by their close proximity. (3) Two symmetric binding sites provided by tris(porphyrinatozinc) are expected to bind two tridentate ligands strongly and cooperatively. (4) Dynamic structural change by binding of guest molecules may induce a change of electronic structure in the hexaporphyrin. This property may be interesting in view of "ligand-induced molecular devices".

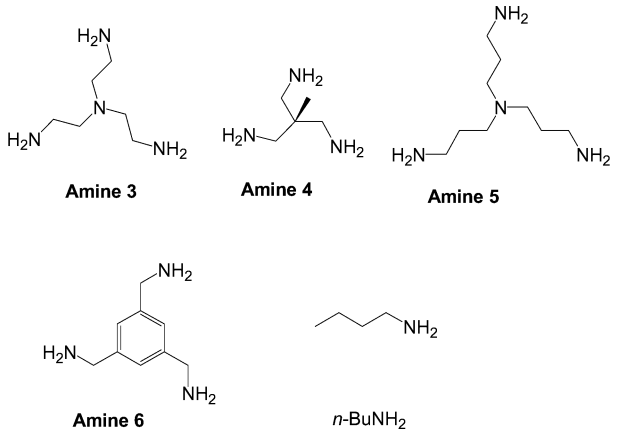

Figure 2. Structures of guest amines.

Before starting the experiment, the sizes and shapes of binding sites for complex **2** were estimated by molecular modeling using CPK models and molecular mechanic simulation.[10] Since porphyrins in **2** are directly connected to bipyridine moieties, bipyridine and porphyrin are almost orthogonal to each other as a dominant conformation. Thus, three porphyrins located at the same side (*a* or the reverse) must give a propeller-like structure (see Figure 1a (front view)). When a tridentate guest, such as a triamine, binds to the propeller parts, dynamic conformational change will be induced by rotational movement along the axis of bonds connecting bipyridine and the porphyrins (Figure 1c,d). Triamines **3**−**6** shown in Figure 2 seem to fit the cavity. Conformations of amines **3**−**6** in the corresponding complexes were estimated by molecular mechanics calculation and are shown in Figure 3.

Results

Synthesis of Hexaporphyrin 2. We have already established a general synthetic pathway of 2,2′-bipyridine having two porphyrins by a nickel-mediated homocoupling reaction of the corresponding porphyrin-substituted bromopyridine.[9a]

(8) (a) Rubtsov, I. V.; Kobuke, Y.; Miyaji, H.; K. Yoshihara, *Chem. Phys. Lett.* **1999**, *308*, 323−328. (b) Kobuke, Y.; Miyaji, H.; Ogawa, K. *Supramol. Chem.* **2002**, *14*, 159−170.

(9) (a) Tomohiro, Y.; Satake, A.; Kobuke, Y. *J. Org. Chem.* **2001**, *66*, 8442−8446. Other 2,2′-bipyridines, 1,10-phenanthroline, and terpyridines linking to porphyrin(s) were reported: (b) Sessler, J. L.; Capuano, V. L.; Burrell, A. K. *Inorg. Chim. Acta* **1993**, *204*, 93−101. (c) Cheng, K. F.; Drain, C. M.; Grohmann, K. *Inorg. Chem.* **2003**, *42*, 2075−2083. (d) Allwood, J. L.; Burrell, A. K.; Officer, D. L.; Scott, S. M.; Wild, K. Y.; Gordon, K. C. *Chem. Commun.* **2000**, 747−748. (e) Vannelli, T. A.; Karpishin, T. B. *Inorg. Chem.* **2000**, *39*, 340−347. (f) Linke, M.; Chambron, J.-C.; Heitz, V.; Sauvage, J.-P.; Encinas, S.; Barigelletti, F.; Flamigni, L. *J. Am. Chem. Soc.* **2000**, *122*, (g) Flamigni, L.; Barigelletti, F.; Armaroli, N.; Collin, J.-P.; Dixon, I. M.; Sauvage, J.-P.; Williams, J. A. G. *Coord. Chem. Rev.* **1999**, *190*−*192*, 671−682. 11834−11844. (h) Uyeda, H. T.; Zhao, Y.; Wostyn, K.; Asselberghs, I.; Clays, K.; Persoons, A.; Therien, M. J. *J. Am. Chem. Soc.* **2002**, *124*, 13806−13813.

(10) Cerius 2 software supplied from Accelrys (Ver.4.6/Force Field UNIVERSAL 1.02) was used.

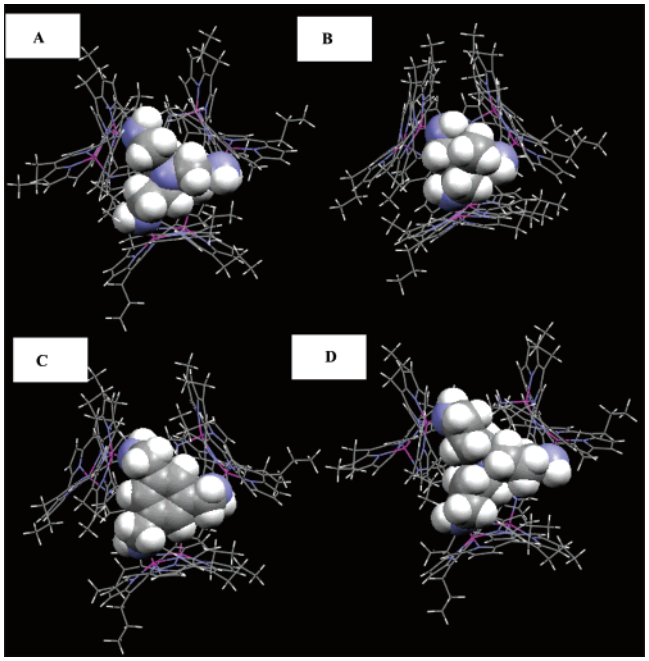

Figure 3. Molecular models of 1:2 complexes of **2** with triamines (a) **3**, (b) **4**, (c) **6**, and (d) **5**. Views are from the *a* side in Figure 1. Only triamine entities were displayed with space-filling shape. Calculated interamine distances are listed in Table 1.

The reaction of 2,2′-bipyridines with two 20-(5,10,15-triheptylporphyrinyl) substituents at the 4,4′-positions with $RuCl_2$ in DMF gave only small amounts of the $Ru(bipy)_3$ complex. It is known that a solvent system containing water is generally required for the successful conversion to $Ru(bipy)_3$. However, the low solubility of the synthesized 2,2′-bipyridine in water hampered the use of such a solvent system. Therefore, we introduced hydrophilic substituents at the meso position of the porphyrin. First, bipyridine bisporphyrin with methoxyethoxyethoxycarbonyl substituents (**1**) was prepared. Condensation of dipyrromethane **9** with bromopyridine aldehyde **7** and ester aldehyde **8**, followed by oxidation with *p*-chloranil, gave a mixture of bromopyridylporphyrin **10**, 5,15-bis(bromopyridyl)porphyrin, and tetraester porphyrin (Scheme 1). The desired product **10** was separated by silica gel column chromatography in 5% yield. After introduction of zinc, a nickel-mediated homocoupling reaction of **11** took place under argon atmosphere to afford bipyridine bisporphyrin **1** in 62% yield. Then, 3 equiv of bipyridine **1** and $Ru(DMSO)_4Cl_2$ were heated in ethylene glycol/H_2O (9:1) at 150 °C to yield the ruthenium trisbipyridine complex accompanied by the bisbipyridine complex as a byproduct. During the reaction, however, transesterification at the side arms of the porphyrins when ethylene glycol was used as solvent was also observed. Thus, the MALDI-TOF mass spectrum (Supporting Information Figure 1) showed the corresponding desired peak, *m*/*z* 5935 (M), along with *m*/*z* 5876 (M − $CH_2CH_2OCH_2$, M − 59) and 5817 (M − $(CH_2CH_2OCH_2)_2$, M − $(59)_2$) in which some values from the methoxyethoxyethoxy group are replaced by those from the hydroxyethoxy group. Therefore, a transesterification reaction using diethylene glychol monomethyl ether in the presence of distannoxane catalyst[11] was

Scheme 1. Synthetic Routes to Zinc(II) Porphyrin **1** and Complex **2**

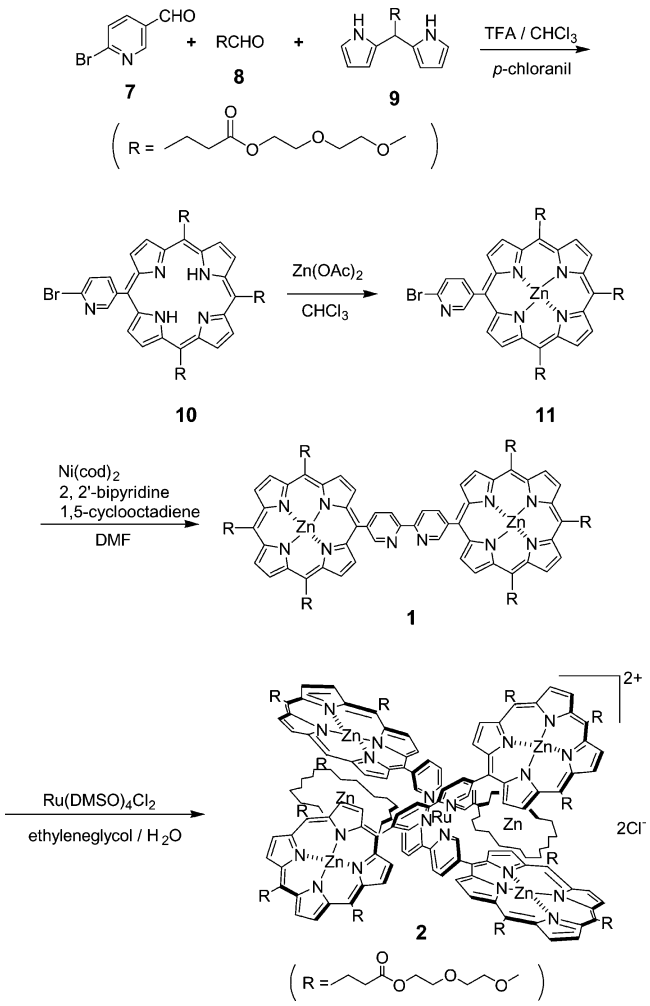

carried out to force all the ester moiety to the methoxyethoxyethoxy group again. The product was separated by silica gel column chromatography twice using two different eluent systems ($CHCl_3$/MeOH/LiBr and CH_3CN/H_2O/NaCl) to give the $Ru(bipy)_3$ type hexaporphyrin **2** in 55% yield. GPC analysis[12] (Supporting Information Figure 2) of **2** showed a single elution peak, suggesting that no porphyrin derivatives of different size, such as a bisbipyridine complex or **1**, had been included. From mass spectroscopic analysis, the obtained compound contained approximately 10% of the mono(hydroxyethoxy) compound[13] that could no longer be converted by transesterification, and the mixture was used as hexaporphyrin **2** for later characterizations.

UV−Vis and Fluorescence Spectra. To examine electronic interaction of closed porphyrins in **2**, the UV−vis spectrum of hexaporphyrin **2** (1 μM) was compared with those of bisporphyrin **1** (3 μM) and $Ru(bipy)_3$ **12** (1 μM) (Supporting Information Figure 3). It was recognized that the spectrum of hexaporphyrin **2** did not correspond to the sum of those of **1** and $Ru(bipy)_3$ **12**. Both the Soret and Q

(11) Otera, J.; Danoh, N.; Nozaki, H. *J. Org. Chem.* **1991**, *56*, 5307−5311.
(12) Conditions: column, Tosoh TSKgel GMH_{HR}-M; eluent, $CHCl_3$:MeOH = 98:2 containing 10 mM LiBr; flow rate, 0.8 mL/min.
(13) This ratio was determined by the intensity of each component in MALDI-TOF MS.

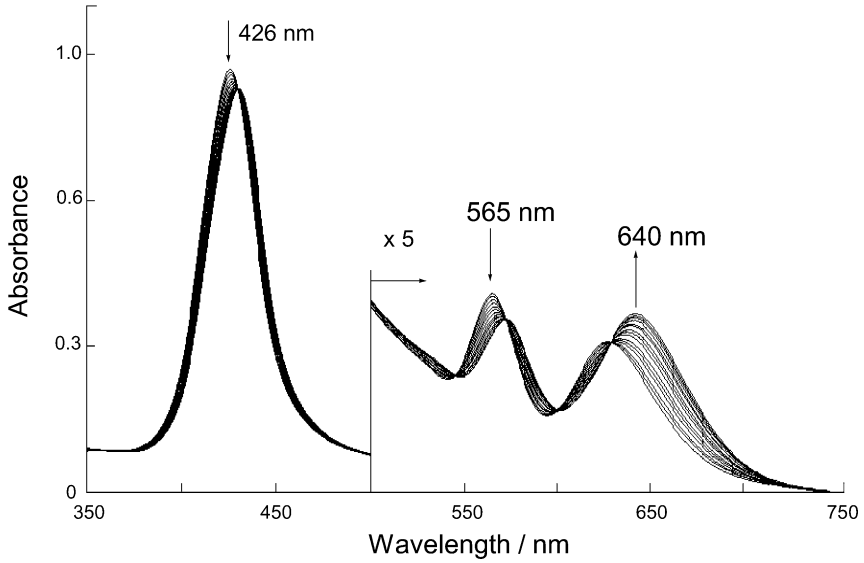

Figure 4. UV−vis spectral changes of **2** upon addition of *n*-BuNH$_2$. Conditions: [**2**] = 1×10^{-6} M in $CHCl_3$, [*n*-BuNH$_2$]/[**2**] = 0, 40, 100, 200, 300, 400, 600, 800, 1000, 1300, 1600, 2000, 2500, 3000, and 3500.

bands of **2** broadened, and maximum peaks of the Q band shifted to longer wavelength compared with those of the Q band of **1**. This behavior is very similar to those of complexation of *meso*-phenylporphyrin-substituted 2,2′-bipyridine with Ni(II), Cu(II), and Pd(II).[9c] Therefore, the spectral change seems to be mainly caused by electronic communication between two porphyrins connected through metal-coordinated 2,2′-bipyridine. Less effect of interaction among other neighboring porphyrins was observed. The fluorescence intensity of complex **2** was decreased to 10% of that of bisporphyrin **1** (Supporting Information Figure 4). This quenching effect may arise from electron transfer from the excited porphyrin to the Ru(bipy)$_3$ unit, similar to the cases of porphyrin complexes linked to a ruthenium complex.[14]

Specific Binding of Triamines with Complex 2. UV−Vis and Fluorescence Spectra. As described in the Design and Molecular Modeling section, some tridentate ligands seem to fit the binding sites provided by hexaporphyrin complex **2**. Therefore, complexation behavior with four different triamines was examined, with use of *n*-butylamine as a reference (Figure 2). Amines **3**−**5** have different arm lengths from the central atom. They are relatively flexible, and their conformation will be variable to fit the space of host molecules. On the other hand, triamine **6** provides a rigid structure by its aromatic ring. The binding behavior was monitored by UV−vis spectroscopy. When monodentate *n*-butylamine was titrated, the Soret (426 nm) and Q (565 and 627 nm) bands were shifted to longer wavelengths, 429, 571, and 640 nm, respectively. These red-shifted values are within the standard range observed normally for coordination of amines to simple zinc porphyrins[15] (Figure 4). Since six porphyrins locate at close distances in complex **2**, the first to sixth binding constants possibly influence one another. However, a Hill coefficient of 1 obtained by analysis of Hill plots (Supporting Information Figure 5) indicates no cooperativity. Thus, coordination of six *n*-butylamines to six porphyrin sites should be independent. The assumption of six independent binding constants for *n*-butylamine gave a value of 1250 M^{-1} by curve-fitting analysis. Compared with that of the *n*-butylamine, the binding affinities of triamines **3**−**6** were higher. Titrations with triamines were carried out for a 1×10^{-6} M solution of hexaporphyrin **2** in $CHCl_3$. UV−vis spectral changes on the addition of triamine **3** are shown in Figure 5. The Soret band was red-shifted from 426 to 432.5 nm, and its absorbance was decreased by ca. 22%. This decrease was significantly larger than that (6%) for *n*-butylamine complexation, suggesting strong interaction in the organized porphyrin space. Two Q bands were also red-shifted from 565 and 627 to 582 and 660 nm, respectively, and the absorbance of the lower energy side was characteristically increased. When changes in the absorbances at 426 and 660 nm were plotted as a function of amine **3** equivalents (Figure 6a), clear bending points were observed at 2 equiv of amine **3**, with a sigmoidal curve raising supposition of positive allosteric binding behavior. A Job plot also indicated the formation of a 1:2 complex (Figure 6b). Titration experiments using amines **4**−**6** were also undertaken. The stoichiometries and the respective binding constants were evaluated from Job plots and titration curves, respectively (Supporting Information Figures 6−9). In all cases, the stoichiometry of complex **2** and triamines **3**−**6** was 1:2. Therefore, the first binding constant of triamine, K_1, and the second one, K_2, were defined as in eq 1, where S = porphyrin

$$K_1 = [SL]/\{[S][L]\}, \quad K_2 = [SL_2]/\{[SL][L]\} \qquad (1)$$

Ru complex **2**, L = triamine, SL = 1:1 complex of **2** and triamine, and SL_2 = 1:2 complex. K_1 and K_2 were determined by computer-assisted curve-fitting analysis[16] (Table 1), and theoretical curves using these values are shown in Supporting

(14) (a) LeGourrierec, D.; Andersson, M.; Davidsson, J.; Mukhtar, E.; Sun, L.; Hammarström, L. *J. Phys. Chem. A* **1999**, *103*, 557−559. (b) Flamigni, L.; Armaroli, N.; Barigeletti, F.; Balzani, V.; Collin, J.-P.; Dalbavie, J.-P.; Heitz, V.; Sauvage, J.-P. *J. Phys. Chem. B* **1997**, *101*, 5936−5943.

(15) Nappa, M.; Valentine, J. S. *J. Am. Chem. Soc.* **1978**, *100*, 5075−5080.

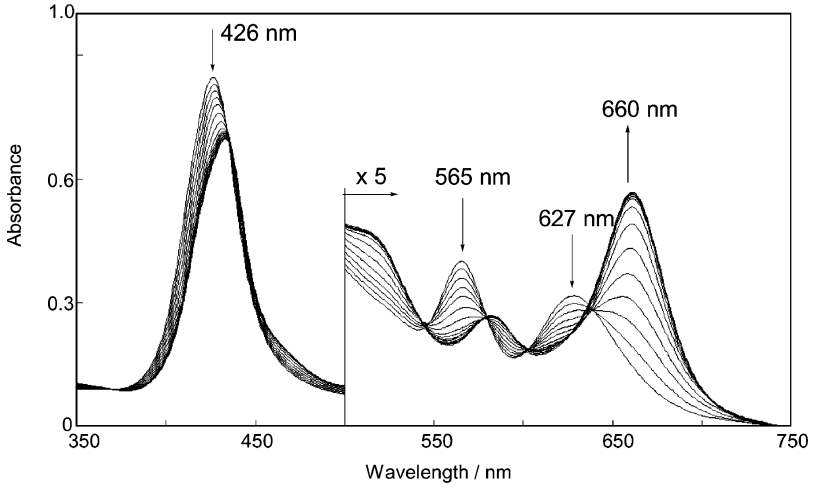

Figure 5. UV−vis spectral changes of **2** upon addition of amine **3**. Conditions: [**2**] = 1 × 10^{-6} M in $CHCl_3$, [amine **3**]/[**2**] = 0, 0.25, 0.5, 0.75, 1, 1.25, 1.5, 1.75, 2, 2.25, 2.5, 3, 4, 6, 8, and 10.

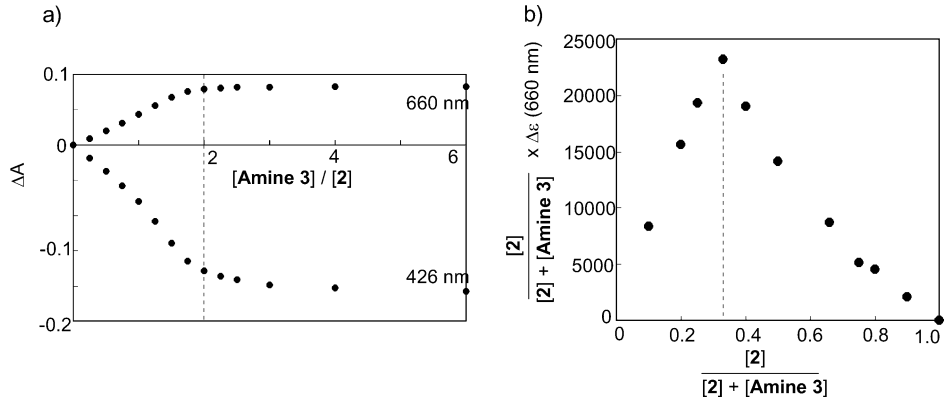

Figure 6. (a) Changes of the absorbance (Δ*A*) of **2** upon addition of amine **3**. (b) Job's plots for the **2**/amine **3** complexation. [**2**] + [amine **3**] = 4 × 10^{-6} M (constant).

Table 1. Sizes, Binding Constants, Effective Molarities, and Cooperativity Factors of Complex **2** with Triamines **3**−**6**

	3	**4**	**5**	**6**
distance between two amino groups[a] (nm)	0.647	0.412	0.766	0.620
K_1[b] (M^{-1})	3.0 × 10^8	2.0 × 10^7	3.5 × 10^6	2.9 × 10^6
EM_1[c] (M)	0.39	0.10	0.042	0.075
K_2[d] (M^{-1})	3.0 × 10^7	1.4 × 10^6	6.0 × 10^6	1.2 × 10^6
EM_2[e] (M)	0.12	0.027	0.055	0.025
$\alpha = 4K_2/K_1$[f]	0.4	0.28	6.9	1.66

[a] Mean distance between two amino groups in each 1:2 complex whose stable structure was calculated by Cerius 2.46 software. [b] First constant of binding with triamine. [c] Effective molarity for the first triamine. [d] Second constant of binding with triamine. [e] Effective molarity for the second triamine. [f] Cooperativity factor for the 1:2 complex.

Information Figures 6−9. In the analysis of 1:2 complexation by UV−vis titration, it is generally difficult to know the $\Delta\epsilon_1$ value, which is the difference between the extinction coefficients of the free host and the intermediate 1:1 complex, while $\Delta\epsilon_2$, the difference between the extinction coefficients of the free host and the final 1:2 complex, can be obtained by adding excess amounts of guests. If the electronic structures of the first and second host/guest complexes are similar, the relationship $^1/_2\Delta\epsilon_1 = \Delta\epsilon_2$ is satisfied. During analysis of complexes with amines **4**−**6**, this relationship could be applied to make well-fitted theoretical curves. In the case of **3**, however, a relationship, $^1/_5\Delta\epsilon_1 = \Delta\epsilon_2$, must be introduced to satisfy finally the experimental result. This nonlinear behavior for the extinction coefficient of the complex with **3** indicates that the electronic structure of the trisporphyrin/amine **3** moiety of the 1:1 complex is varied dramatically by the formation of the 1:2 complex. Therefore, the sigmoidal curve observed in Figure 6a was not caused by the positive allosterism on the binding behavior, but through nonlinearity of the extinction coefficient.

Since hexaporphyrin **2** has two tritropic binding sites, the thermodynamic effective molarity[17] for each tritropic (EM) site and the cooperativity factor (α) for two binding sites must be considered when the chelation and allosteric effects are estimated. These are defined by eqs 2 and 3, and the

$$EM_L = \{(K_{L(1)L(2)L(3)}/K_{L(1)}{}^3)\}^{1/2} \quad (2)$$

$$\alpha = 4K_2/K_1 \quad (3)$$

values evaluated are also listed in Table 1. In eq 2 EM_L is an effective molarity, $K_{L(1)L(2)L(3)}$ is a binding constant of the

(16) Conners, K. A. *Binding Constants*; John Wiley: New York, 1987.

(17) (a) Kirby, A. J. *Adv. Phys. Org. Chem.* **1980**, *17*, 183−278. (b) Sanders, J. K. M. Templated Chemistry of Porphyrin Oligomers. *Comprehensive Supramolecular Chemistry*; Pergamon Press: Oxford, 1996; Vol. 9, pp 131−164. (c) Anderson, H. A.; Anderson, S.; Sanders, J. K. M. *J. Chem. Soc., Perkin Trans. 1* **1995**, 2231−2245.

tritropic host and triamine, and $K_{L(1)}$ is the first constant of binding of one amino group in the triamine to the tritropic host. Similarly, $K_{L(2)}$ and $K_{L(3)}$ are defined as the second and third binding constants of other amino groups in the triamine. Since $K_{L(1)}$ cannot be determined directly, the binding constant of *n*-butylamine, $K = 1250\ M^{-1}$, was used as $K_{L(1)}$. In the case of complex **2** and triamines, two effective molarities, EM_1 and EM_2, can be obtained. They are defined as the first and second effective molarities for the first and second triamines, respectively.

In eq 3 α is a cooperativity factor for the 1:2 complex, K_1 is the first binding constant of the triamine to compound **2**, and K_2 is the second binding constant.

When we compare a series of aliphatic triamines **3**−**5**, having triethylamino, trimethylamino, and tripropylamino groups, respectively, the binding constants (K_1 and K_2) are in the following orders: amine **3** > **4** > **5** for K_1 and amine **3** > **5** > **4** for K_2. K_2 is much smaller than K_1 in the cases of amines **3** and **4**, while a reverse order is observed for amine **5**. Effective molarity is convenient to estimate the strain and chelate effects in a multibinding host/guest pair. Since all effective molarities of EM_1 and EM_2 are below 1 M, $K_{L(2)}$ and/or $K_{L(3)}$ are smaller than $K_{L(1)}$. This result indicates that some strain and/or small chelate effects are given in host/guest complexation. Complex **2** must open its "mouth" to accept a triamine at the central pore, and the motion accompanies torsions of bonds between porphyrins and bipyridines. Dihedral angles of 1:2 complexes of **2** with amines **3**−**5** between porphyrin and bipyridine were estimated by molecular mechanic calculation as 121.5°, 131.6°, and 119.1°, respectively. Thus, the degree of torsion from the orthogonal conformation (dihedral angle 90°) is largest for the smallest triamine **4** and decreases in the order of increasing size, **4** > **3** > **5**. This torsion may decrease the effective molarities. Since a twisted conformation takes a higher energy state compared with that of an orthogonal one, strain energy must work in complexes of **2** with triamines. The chelate effect of triamines and stabilization energies of three nitrogen/zinc coordinations compensate for the strain energy. Relatively large effective molarities of complexes **2** with **3** ($EM_1 = 0.39$ M and $EM_2 = 0.12$ M) indicate that distortion is more or less counterbalanced by the chelate effect, whereas amine **5** having more methylene units has a smaller chelate effect ($EM_1 = 0.042$ M and $EM_2 = 0.055$ M), and the shorter amine **4** receives significantly high torsional energy on binding of the second triamine ($EM_1 = 0.10$ M and $EM_2 = 0.027$ M). Amine **3**, having triethylamino groups, seems the guest molecule best able to be accommodated among the aliphatic triamines. Although amine **6** has interamine distances similar to those of amine **3** (Figure 3), its binding affinity is much less than that of amine **3**, suggesting that hexaporphyrin **2** can discriminate not only the size but also the shape of the guest molecules. It is noteworthy that information on the torsion at the first site is transmitted to another site at a separation distance of 13.5 Å.[18] From molecular modeling, two binding sites must twist in opposite directions to each other to accept two triamines (Figure 1). Since these two binding sites are connected through a rigid $Ru(bipy)_3$ moiety, one torsional motion induced by the first binding of triamine affects the conformation of another binding site at the opposite side. Depending on the structure of the amine, the second binding is associated with negative or positive cooperativity. In the case of amines **3** and **4**, negative cooperativity was observed. On the other hand, positive cooperativity was observed for the binding of amine **5**, suggesting that the conformation induced at the opposite binding site was preorganized suitably for accommodating **5**.

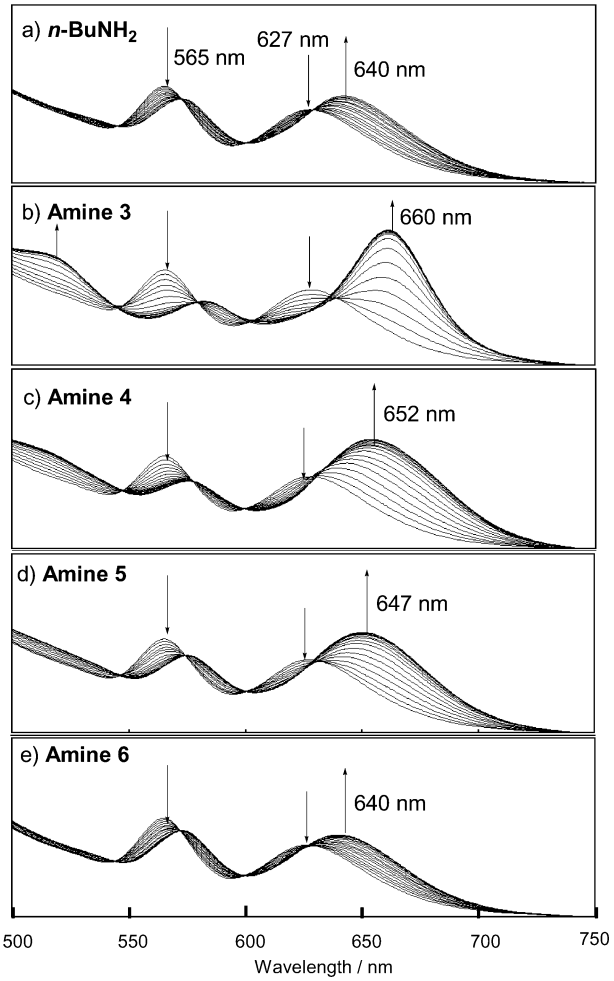

Figure 7. UV−vis spectral changes of **2** (1×10^{-6} M) upon addition of amine derivatives.

As described above, complex **2** could recognize subtle structural differences between triamines, and amine **3** was found to be the best fit guest from the comparison of their binding constants. Interestingly, several spectroscopic data of the 1:2 complex of **2** with **3** were really characteristic. In Figure 7, the titration behavior of the Q band region is compared. Coordination of an alkylamine to monomeric zinc porphyrin is known to produce generally a red shift of the Q(0,0) band by ca. 19 nm.[15] The coordination of *n*-butylamine gave a red shift of 13 nm for complex **2**. The largest red shift (33 nm) was observed for amine **3**, and intermediate red shifts of 20−25 nm were observed for amines **4** and **5**, while **6** shifted by only 13 nm. The relative

(18) The distance between two tertiary amines in the 1:2 complex of **2** with triamine **3** was calculated.

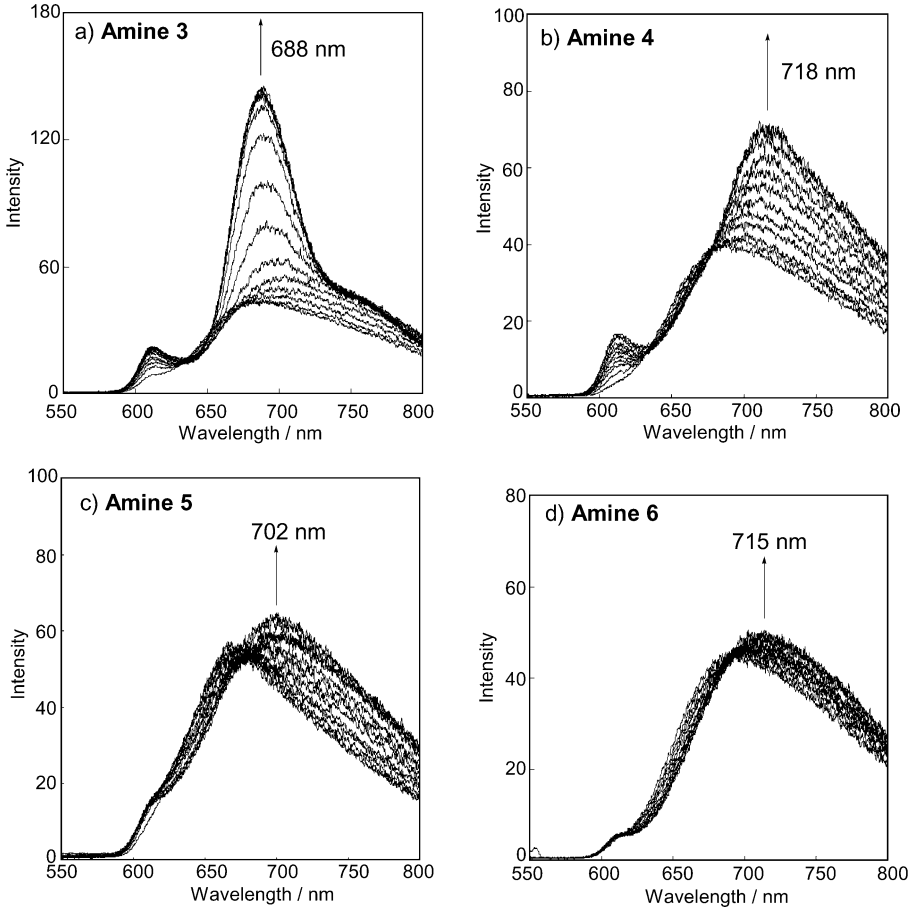

Figure 8. Fluorescent spectral changes of **2** (5×10^{-7} M in $CHCl_3$) upon addition of triamine derivatives: (a) amine **3**, $\lambda_{EX} = 433$ nm (absorbance 0.408−0.412), (b) amine **4**, $\lambda_{EX} = 440$ nm (absorbance 0.283−0.281), (c) amine **5**, $\lambda_{EX} = 430$ nm (absorbance 0.402−0.413), (d) amine **6**, $\lambda_{EX} = 430$ nm (absorbance 0.407−0.393).

order of shift values was the same as that of the intensity increases of the Q(0,0) bands. Fluorescence spectra of complex **2** with a series of these amines also gave a characteristic tendency. Although the fluorescence intensity of hexaporphyrin **2** was relatively small, it was useful to monitor the fluorescence intensities of the complexes (Figure 8). To detect weak luminescence, the sensitivity of the photomultiplier was raised significantly from the standard value. Since all the complexation behavior did not show any isosbestic point, we chose as excitation wavelengths those points at which the change of absorption was smallest. Each wavelength and the range of absorption intensity are described in Figure 8. When amines **5** and **6** were added gradually to hexaporphyrin **2** (5×10^{-7} M in $CHCl_3$), the maximum peaks were shifted to longer wavelengths until reaching 715 and 702 nm, respectively, without an increase in the intensity. In the case of amine **4**, a small increase in the intensity was accompanied by a longer wavelength shift, and further, a relatively larger increase in the intensity was observed for amine **3**. Relationships between the amount of added amines **3**−**6** and the fluorescence intensity at each peak maximum are illustrated in Figure 9. This figure clearly shows specific behavior for amine **3**. Up to 1 equiv of amine **3** the behavior was similar to that of the others, but the intensity was increased sharply by the formation of the 1:2 complex.

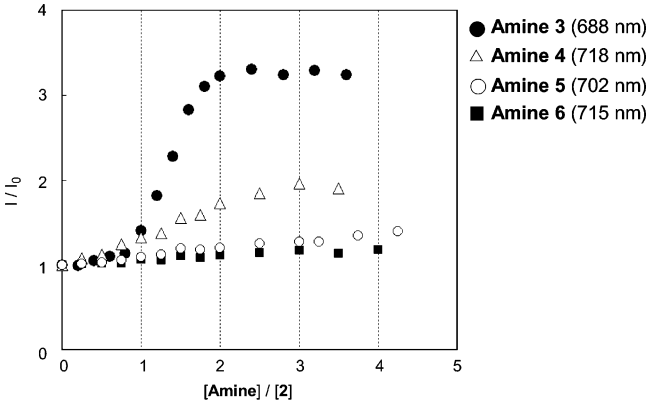

Figure 9. Changes of the relative fluorescence intensity (I/I_0) of **2** (5×10^{-7} M in $CHCl_3$) upon addition of amines **3**−**6**.

Isothermal Titration Calorimetry (ITC).[19] The special characteristic of the 1:2 complex with amine **3** was observed also in isothermal calorimetric studies. ITC profiles at 25 °C for the titration of hexaporphyrin **2** (4×10^{-5} M) with amines **3** and **4** are shown in Figure 10. Each of the heat burst curves corresponds to the injection (5 μL) of amine solution (1.7 mM). The areas under these heat burst curves were determined by integration to yield the injection heats.

(19) Wiseman, T.; Williston, S.; Brandts, J. F.; Lin, L.-N. *Anal. Biochem.* **1989**, *179*, 131−137.

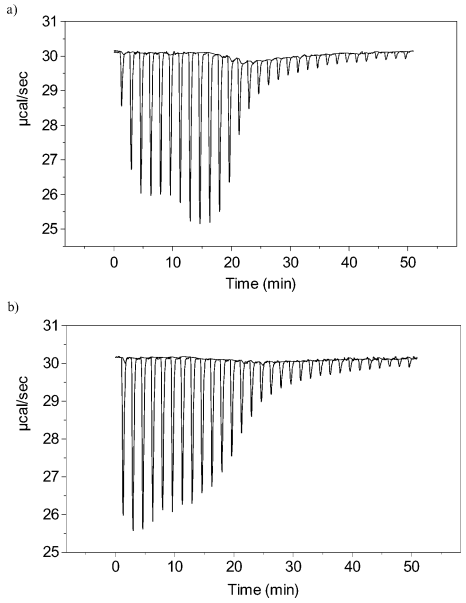

Figure 10. ITC profiles for the titration of hexaporphyrin **2** (4×10^{-5} M) with amines (a) **3** and (b) **4** (1.7 mM in syringe, 5 μL per injection) at 25 °C.

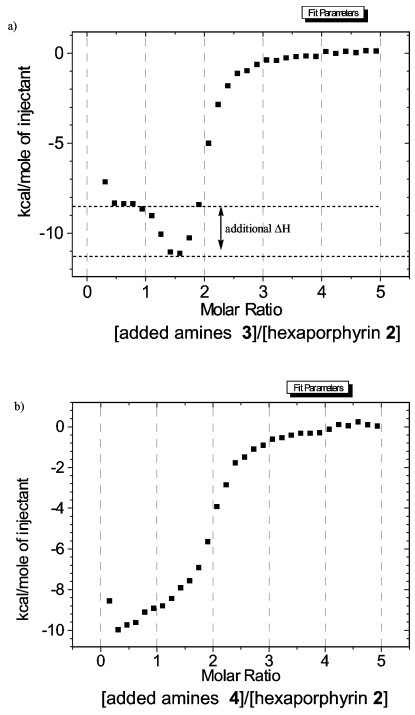

Figure 11. Corrected injection heats plotted as a function of the molar ratio [added amines **3** (a) or **4** (b)]/[hexaporphyrin **2**].

These heats were corrected by subtracting the dilution heats derived from the $CHCl_3$ injection. The corrected injection heats were plotted as a function of the molar ratio, [added amine **3** or **4**]/[hexaporphyrin **2**], and are shown in Figure 11. Parts a and b both clearly show that complex **2** forms 1:2 complexes with triamine **3** or **4**. In the case of amine **3**, 8.2 kcal/mol of injection heat was observed on the addition of 1 equiv of amine, and then the value increased to 11.1 kcal/mol on adding the second equivalent. In the case of **4**, the injection heat decreased monotonically from 10 kcal/mol in the whole titration range. Since binding constants with amine **3** were obtained by UV−vis titration as $K_1 = 3.0 \times 10^8$ M^{-1} and $K_2 = 3.0 \times 10^7$ M^{-1}, the amine injected must be bound completely in the presence of a 4×10^{-5} M solution of complex **2**. Therefore, the observed values 8.2 and 11.1 kcal/mol correspond to ΔH_1 and ΔH_2, respectively. The additional heat observed on the second binding suggests that the 1:2 complex formation with amine **3** is favored in the enthalpy term. On the contrary, no stabilizing effect was observed in the case of **4**. Although we tried to estimate the binding constants from the ITC results, no reliable data were obtained because the binding was too strong under the conditions.

NMR Spectra. The proton NMR spectrum of bisporphyrin **1** showed clear sharp signals assignable to the characteristic β protons on pyrrole, bipyridine, and α-methylene substituents in meso positions as indicated in Figure 12. In the case of complex **2**, signals of β protons on pyrrole may exist in the area between 10.2 and 8.8 ppm as partially broad and unclear peaks, and those of α-methylene occur around 6−5 ppm as very broad signals. These signals did not show any sharpening in the temperature range of +100 to −40 °C. When amine **3** was titrated up to 2 equiv, these broad signals were converted to clear and sharp ones, and the coordinated two triamines were observed between −2.8 and −7.6 ppm. The latter signals could be assigned as NH_2 (−5.79 and −7.42 ppm), α protons of *tert*-nitrogen (−2.76 and −5.35 ppm), and β protons of *tert*-nitrogen (−4.68 and −5.09 ppm) by exchange reaction with d_4-methanol and H−H COSY and HMQC measurements (Supporting Information Figure 10). These large upper field shifts indicate that two triamines **3** locate in the center of the triangular porphyrin pockets. Further, it was recognized that six porphyrin and pyridine groups were equivalent, and eight β protons on each porphyrin were different from each other. Assignment of the β protons on pyrrole and the bipyridyl protons was performed as follows. Since β carbons of the pyrrole entity are known to appear around 130 ppm, eight β protons on pyrrole were assigned from H−C correlation (HMQC) spectra. Similarly, Py_3 and Py_4 were assigned from HMQC spectra (Supporting Information Figure 11). Then, coupling pairs were determined by H−H COSY and TOCSY (Supporting Information Figure 12).[20] Finally, each pair was assigned by NOE experiments. In the complex with amine **3**, strong NOE signals were observed, and the corresponding protons were assigned without contradiction with due consideration of molecular modeling. In particular, very strong NOE signals were observed between β_2 and Py_4 and between β_3 and Py_6 (Figure 13). The result shows that the torsional angle between the pyridine and porphyrin planes becomes small and the corresponding distances between the two interacting protons are shortened. Further, a clear NOE signal was observed between β_1 and β_6, supporting the triangular structure shown in Figure 1. The NOE correlations observed are listed in Table 2 and shown in Figure 14. Since the intensity of the NOE signals is proportional to the inverse sixth power of

(20) Since the coupling constant between β protons on the pyrrole ring is relatively small (<2 Hz) in complex **2**, TOCSY is also effective to obtain coupling pairs.

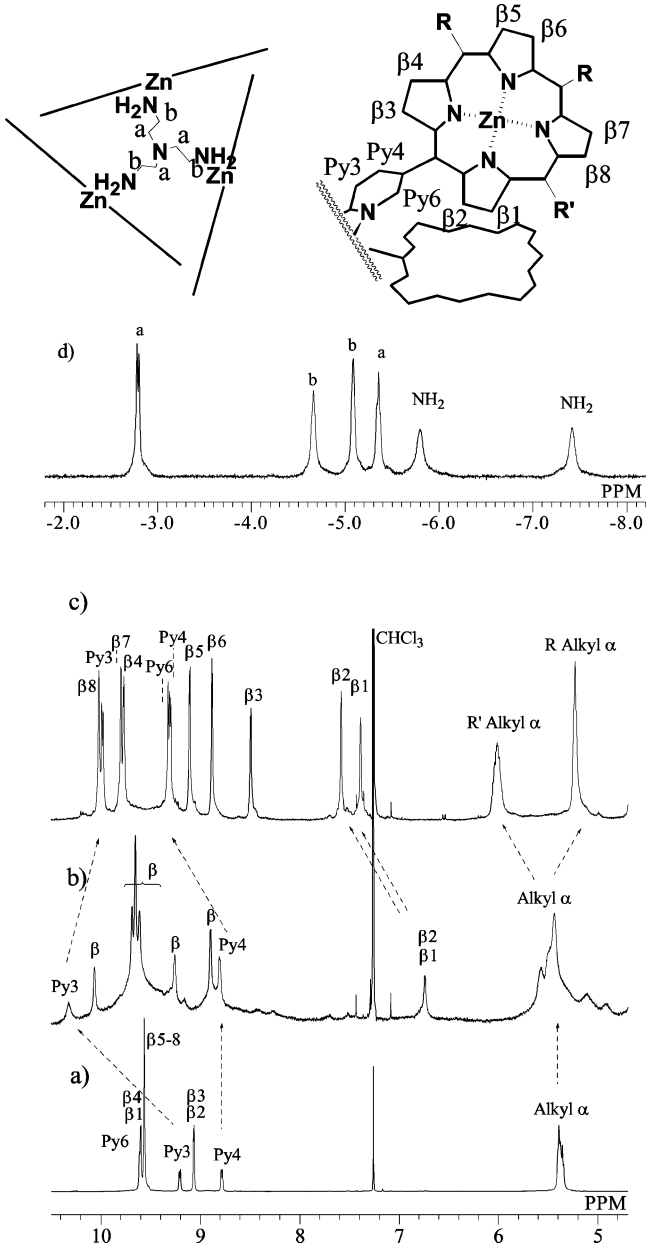

Figure 12. ^{1}H NMR spectra (selected areas) of (a) bisporphyrin **1**, (b) complex **2**, and (c, d) a 1:2 complex with amine **3** ((a−c) from 11 to 4.6 ppm, (d) from −1 to −9 ppm).

the distance,[21] distances between β_2 and Py_4 (2.1 Å), β_3 and Py_6 (2.1 Å), and β_1 and β_6 (2.7 Å) were estimated.[22]

The ^{1}H NMR spectra of the 1:2 complexes with amines **4** and **5** were also measured (Figure 15), but the complete assignments were difficult because of broadened signals and their small intensities in the correlation spectra. These broadenings may be caused by inhomogeneity of complexes with amine **4** and, especially, amine **5**. The degree of peak sharpness followed the same order of the relative strength of the binding constant (K_1), **3** > **4** > **5**. Although detailed peak assignment of the complexes with amines **4** and **5** was not accomplished, peak(s) that appeared at the highest field position may be assigned as NH_2 of bound amines **4** and **5**. The highest peaks of the complexes with amines **4**, **3**, and **5** appeared at −7.85, −7.45, and −4.78 ppm, respectively, and the order followed the reverse of the molecular sizes (**4** < **3** < **5**; see Table 1). This result suggests that complex **2** adjusts its size and shape to fit guest molecules as we expect at the stage of molecular design.

Discussion

We understand that triamine **3** is an excellent guest for complex **2**. All the data indicated that its 1:2 complex with amine **3** is special compared with other 1:2 complexes with triamines **4**−**6**, and it is not a simple duplication of the "1:1 complex with amine **3**." One of the distinctive features is its rigidity. In general, rigid molecules show small Stokes shifts, and their fluorescence intensities are relatively large because the nonradiative transition based on molecular vibration is suppressed. In Table 3, the wavelengths and half-bandwidths of the Q(0,0) bands of all the 1:2 complexes are listed with their Stokes shifts. It is clear that the half-bandwidth and the Stokes shift of the complex with triamine **3** are significantly smaller than those of the others. A narrow half-bandwidth indicates that there are smaller numbers of vibrational frequency states at the lowest excited state, and a small Stokes shift indicates that the nuclear reorganization between ground and excited states is small. A sudden change of the fluorescence intensity in the course of titration shown in Figures 8a and 9 suggests that a rigid structure different from the 1:1 complex is produced in the formation of the 1:2 complex. Another characteristic feature was observed in the additional heat of formation of the 1:2 complex with triamine **3** in calorimetric titration studies. Since the constant K_1 of association with triamine **3** is larger than its K_2, the total free energy change must follow the order $-\Delta G_1 > -\Delta G_2$. However, a reverse order, $-\Delta H_2 > -\Delta H_1$, was clearly observed in the titration experiment. Therefore, a larger negative entropy term $T\Delta S_2$ must outweigh the favorable enthalpy term. Although exact values of ΔG, ΔH, and ΔS could not be obtained by ITC because the binding affinity is too strong, the qualitative relationship suggests that 1:2 complex formation of amine **3** is suppressed only by the restricted molecular motion.

Some enthalpic stabilization must occur in forming the 1:2 complex with **3**. To account for the source of the additional heat of formation in ITC and large red shift observed in the UV−vis spectrum, we consider two possibilities. One is stabilization by overlapping of π-orbitals between distorted porphyrin and bipyridine units. In-plane nuclear reorganization (IPNR) is another possibility. IPNR was introduced by Shelmutt et al.[23] to explain large red shifts of distorted porphyrins. It is defined by the changes in the porphyrin bond lengths and bond angles induced by interactions between the substituent and the porphyrin macrocycle.

(21) *Encyclopedia of Nuclear Magnetic Resonance*; Grant, D. M., Harris, R. K., Eds.; John Wiley & Sons: New York, 1996; Vol. 5, pp 3290−3301.

(22) The relationship between the intensity of differential NOEs and the distance (2.6 Å) of pairs of β protons coupled to each other ($\beta_1-\beta_2$, $\beta_3-\beta_4$, $\beta_5-\beta_6$, $\beta_7-\beta_8$) was used as the standard in each analysis.

(23) Haddad, R. E.; Gazeau, S.; Pecaut, J.; Marchon, J.-C.; Medforth, C. J.; Shelnutt, J. A. *J. Am. Chem. Soc.* **2003**, *125*, 1253−1268.

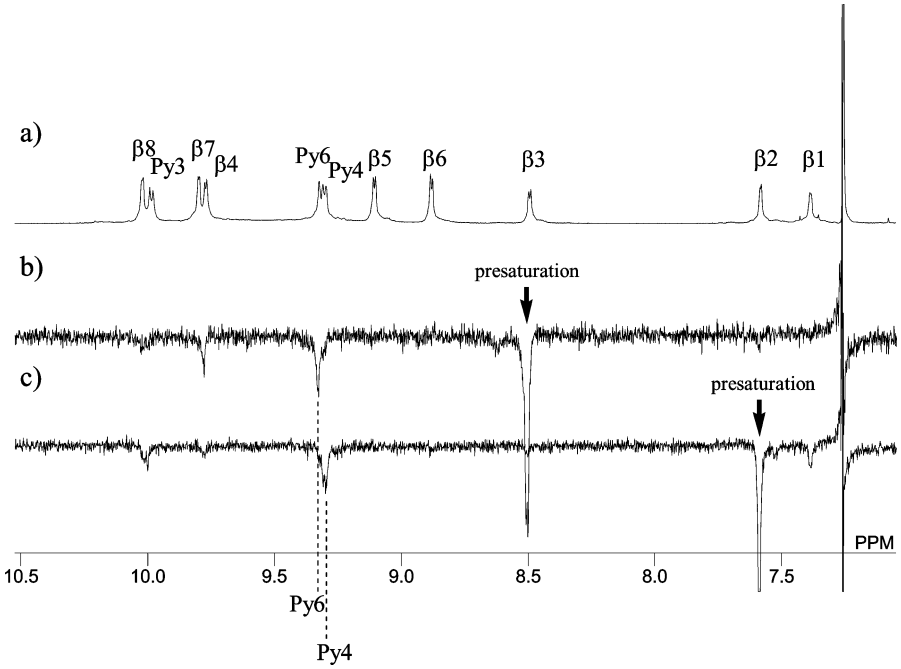

Figure 13. ^{1}H NMR spectra of complex **2** with amine **3** for differential NOE experiments: (a) base spectrum, (b) on presaturation of β_3, (c) on presaturation of β_2.

Table 2. NOE Enhancements (%) Obtained on Presaturation of Different Protons of the **2**/Amine **3** Complex

	obsd NOE signal												
presaturated	β_1	β_2	β_3	β_5	β_6	β_7	β_4	β_8	Py_3	Py_4	Py_6	R′ [a]	R[b]
β_1	−100	−19.2			−17.7								
β_2	−9.9	−100							−11.4	−42.5			
β_3			−100				−8.8				−34.5		
β_5				−100	−16.9		−11.7						
β_6				−13.7	−100								
β_7 and β_4			−8.7			−100	−100	−16.2				−16.2	−41.8
β_8 and Py_3						−19.5		−100	−100	−15.7		−31.6	−4.6
Py_4 and Py_6		−18.6	−7.4						−21.5	−100	−100		

[a] R′ = α-methylene protons of R′. [b] R = α-methylene protons of R.

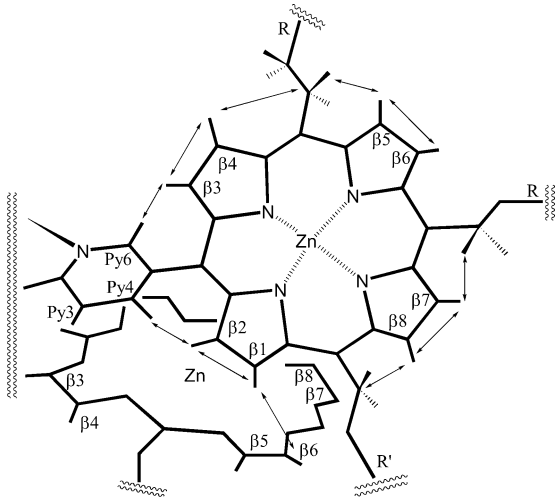

Figure 14. NOE correlations observed indicated by arrows.

In the case of the 1:2 complex of hexaporphyrin complex **2** and triamine **3**, the total enthalpy may be favorable by deformation induced by strong binding. However, further data, such as precise nuclear coordinates from X-ray structural determination and supporting molecular calculation, are certainly necessary to identify the contribution.

Conclusion

We have established an efficient method for the synthesis of M(bipy)$_3$ type hexaporphyrin complex **2**. Since this method can be applied to various trisbipyridine metal complexes and metalloporphyrins, systematic studies using these multiporphyrin complexes will be possible. Further, we found an excellent combination of complex **2** and triamine **3**. This highly specific molecular recognition and strong affinity were accompanied by the dynamic structural change of six porphyrins, and the differences were clearly detected by various spectroscopic measurements and ITC studies. These features will be developed as a molecular switch and a machine induced by specific ligation.

Experimental Section

5,10,15-Tris{methoxy(ethoxy)$_2$carbonylethyl}-20-(2′-bromo-5′-pyridyl)porphyrin (10). Aldehyde **7** (0.90 g, 4.8 mmol), aldehyde **8** (0.98 g, 4.8 mmol), and dipyrromethane **9** (3.1 g, 9.7 mmol) were dissolved in 970 mL of chloroform. After the solution was purged with N_2 for 10 min, trifluoroacetic acid (1.2 mL, 16.9 mmol) was added, and the mixture was stirred in the dark for 6 h at room temperature. Then *p*-chloranil (4.0 g) was added, and the crude mixture stirred further for 6 h. The mixture was added to a

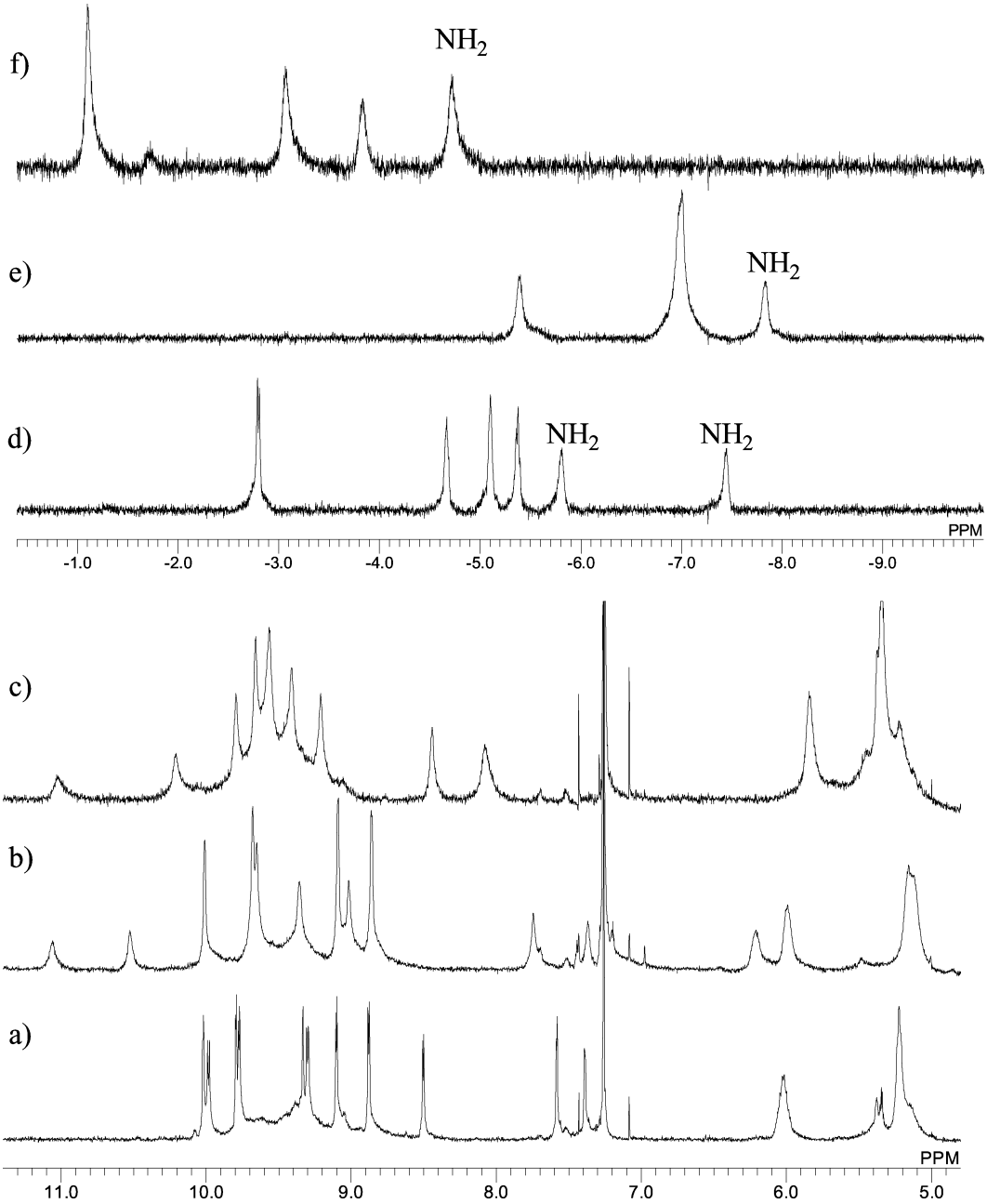

Figure 15. ^{1}H NMR spectra of 1:2 complexes of **2** with amines (a, d) **3**, (b, e) **4**, and (c, f) **5** in $CDCl_3$.

Table 3. Spectral Data of the 1:2 Complex of **2** with Amines

amine	Q(0,0) absorption/nm (half-bandwidth/nm)	Q(0,0) emission/nm (half-bandwidth/nm)	Stokes shift/ 10^2 cm^{-1}
no amine	627 (66)	680 (145)	13
amine **3**	660 (46)	688 (59)	6
amine **4**	652 (65)	718 (126)	14
amine **5**	647 (71)	702 (143)	12
amine **6**	640 (68)	715 (146)	16

saturated aqueous $NaHCO_3$ solution, and the organic layer was separated. The organic layer was washed with a saturated aqueous $NaHCO_3$ solution and brine, after which it was dried over Na_2SO_4 and concentrated under reduced pressure. The residue was purified twice by column chromatography on silica gel (chloroform:acetone = 10:1). The resulting purple solid was dissolved in a minimum amount of ethyl acetate and reprecipitated by addition of hexane. The purple solid was collected and dried under vacuum to give **10** (215 mg, 5%): ^{1}H NMR (600 MHz, $CDCl_3$) δ 9.61 (d, 2H, J = 4.2 Hz), 9.58 (d, 2H, J = 4.2 Hz), 9.50 (d, 2H, J = 4.2 Hz), 9.14 (d, 1H, J = 2.4 Hz), 8.77 (d, 2H, J = 4.2 Hz), 8.31 (dd, 1H, J = 7.8, 2.4 Hz), 7.94 (d, 1H, J = 7.8 Hz), 5.38 (t, 2H, J = 8.4 Hz), 5.34 (t, 4H, J = 8.4 Hz), 4.38 (t, 2H, J = 4.8 Hz), 4.35 (t, 4H, J = 4.8 Hz), 3.69 (t, 2H, J = 4.8 Hz), 3.66 (t, 4H, J = 4.8 Hz), 3.59−3.48 (m, 12H), 3.39−3.35 (m, 6H), 3.29 (s, 3H), 3.27 (s, 3H), −2.81 (s, 2H); ^{13}C NMR (150 MHz, $CDCl_3$) δ 172.60, 172.57, 153.58, 143.04, 142.00, 137.45, 126.31, 117.55, 117.19, 112.59, 71.77, 70.42, 69.09, 63.96, 63.94, 58.99, 58.97, 42.01, 41.86, 30.81, 30.49 (signals of α and β carbons of pyrroles were missing because of inner NH tautomerizations); MALDI-TOF MS (dithranol) m/z 989.97 $(M + H)^+$, calcd for $C_{49}H_{58}BrN_5O_{12}$ 988.92; UV−vis ($CHCl_3$) λ_{max}/nm (absorbance) 653 (0.020), 595 (0.023), 552 (0.036), 518 (0.081), 419 (1.635).

5,10,15-Tris{methoxy(ethoxy)$_2$carbonylethyl}-20-(2′-bromo-5′-pyridyl)porphyrinatozinc (11). Saturated zinc acetate solution in methanol (4 mL) was added to a solution of **10** (195 mg, 0.197

mmol) in chloroform (20 mL). After being stirred for 2 h at room temperature, the mixture was washed with aqueous $NaHCO_3$ solution (50 mL) and water (50 mL × 2), dried over Na_2SO_4, and evaporated under reduced pressure. The product was dissolved in a minimum amount of ethyl acetate and reprecipitated by addition of hexane. The purple solid was collected and dried under vacuum to give **11** (188 mg, 95%): ^{1}H NMR (600 MHz, $CDCl_3$) δ 9.57 (s, 6H), 9.53 (d, 2H, J = 4.8 Hz), 9.05 (d, 1H, J = 2.4 Hz), 8.79 (d, 2H, J = 4.8 Hz), 8.30 (dd, 1H, J = 7.8, 2.4 Hz), 7.90 (d, 1H, J = 7.8 Hz), 5.40−5.32 (m, 6H), 4.16−4.08 (m, 6H), 3.56−3.48 (m, 6H), 3.27−3.20 (m, 6H), 2.62−2.51 (m, 6H), 2.29−2.15 (m, 6H), 2.09 (s, 6H), 2.04 (s, 3H); ^{13}C NMR (150 MHz, $CDCl_3$) δ 172.86, 153.53, 149.78, 149.74, 149.28, 149.04, 142.96, 141.43, 138.34, 131.41, 129.69, 129.53, 129.48, 126.01, 117.85, 117.57, 117.53, 113.07, 70.48, 70.44, 69.35, 69.33, 68.70, 68.67, 63.69, 57.95, 57.92, 42.39, 42.29, 31.03, 30.96; MALDI-TOF MS (dithranol) m/z 1052.90 $(M + H)^+$, calcd for $C_{49}H_{56}BrN_5O_{12}Zn$ 1052.29; UV−vis ($CHCl_3$) λ_{max}/ nm (absorbance) 600 (0.030), 559 (0.083), 425 (1.971).

5,5′-Bis[5,10,15-tris{methoxy(ethoxy)$_2$carbonylethyl}-porphyrinatozinc(II)]-2,2′-bipyridine (1). Porphyrin **11** (135 mg, 0.128 mmol), 2,2′-bipyridine (26 mg, 0.171 mmol), and 1,5-cyclooctadiene (50 μL, 0.408 mmol) were dissolved in 190 mL of dry DMF in a Schlenk flask under argon atmosphere. After the mixture was stirred for 5 min, $Ni(cod)_2$ (ca. 860 mg, 3.13 mmol) was added, and the reaction mixture stirred at room temperature in the dark. After 24 h, DMF was removed under reduced pressure. The residue was dissolved in chloroform and washed with 5% ethylenediaminetetraacetic acid solution adjusted to pH 12 (50 mL × 5) to remove excess nickel species. The organic layer was dried over Na_2SO_4 and evaporated under reduced pressure. The crude product was purified on a preparative high-pressure liquid chromatograph (Japan Analytical Industry, LC-908) attached to a GPC column (TSK G2500H_{HR} column, TOSOH Co.) eluted with chloroform:pyridine = 4:1. The collected desired product was dissolved in a minimum amount of ethyl acetate and reprecipitated by addition of hexane. The purple solid was collected and dried under vacuum to give **1** (78 mg, 62%): ^{1}H NMR (600 MHz, $CDCl_3$) δ 9.61 (br s, 2H, Py_6) 9.60 (d, 4H, J = 4.2 Hz, β_2) 9.56 (s, 8H, β_3, β_4) 9.21 (d, 2H, J = 7.8 Hz, Py_3) 9.06 (d, 4H, J = 4.2 Hz, β_1) 8.78 (d, 2H, J = 7.8 Hz, Py_4) 5.40−5.32 (m, 12H, a, a′) 4.16−4.08 (m, 12H, c, c′) 3.59−3.52 (m, 12H, b, b′) 3.29−3.25 (m, 12H, d, d′) 2.67−2.61 (m, 12H, e, e′ or f, f′) 2.30−2.26 (m, 12H, e, e′ or f, f′) 2.15 (s, 12H, g) 2.13 (s, 6H, g′); ^{13}C NMR (150 MHz, $CDCl_3$) δ 172.88 (C═O), 172.84 (C═O), 155.05 (Py_2), 153.45 (Py_6), 149.66 (α), 149.51 (α), 149.39 (α), 149.02 (α), 142.05 (Py_4), 139.30 (Py_5), 131.81 (β_1), 129.39 (β_2), 129.25 (β_3, β_4), 119.44 (Py_3), 117.41 (meso), 117.31 (meso), 114.99 (meso), 70.54 (e or f), 70.51 (e′ or f′), 69.42 (e or f), 69.38 (e′ or f′), 68.71 (d), 68.67 (d′), 63.67 (c, c′), 57.97 (g, g′), 42.26 (b, b′), 30.89 (a, a′); MALDI-TOF MS (dithranol) m/z 1945.63 $(M + H)^+$, calcd for $C_{98}H_{112}N_{10}O_{24}Zn_2$ 1944.77; UV−vis ($CHCl_3$) λ_{max}/nm (ϵ) 603 (14950), 561 (31400), 432 (469500), 425 (469550), 315 (36500).

Tris[5,5′-bis[5,10,15-tris{methoxy(ethoxy)$_2$carbonylethyl}-porphyrinatozinc(II)]-2,2′-bipyridine]ruthenium(II) Chloride (2). A solution of $Ru(DMSO)_4Cl_2$[24] (3 mg, 6.3 μmol) and **1** (37 mg, 19.0 μmol) in 4 mL of ethylene glycol (containing 10% water) was heated at 150 °C under nitrogen atmosphere for 30 min. The mixture was cooled to room temperature, and chloroform (10 mL) was added to the mixture. The mixture was washed with water (20 mL × 2). The organic layer was dried over Na_2SO_4 and evaporated under reduced pressure. Diethylene glycol monomethyl ether (5 mL), toluene (2 mL), and distannoxane catalyst[11] (1 mg) were added to the residue, and the mixture was refluxed for 4 h. After the mixture was cooled to room temperature, 10 mL of chloroform was added, and the resulting solution washed with water (20 mL × 2). The organic layer was dried over Na_2SO_4 and evaporated under reduced pressure. The residue was purified by column chromatography on silica gel with gradient elution of chloroform: methanol = 10:1 by addition of 10 mM LiBr/methanol. The fractions containing the desired product were washed with water. The organic layer was dried over Na_2SO_4 and evaporated under reduced pressure. The residue was further purified by column chromatography on silica gel with gradient elution of acetonitrile: water = 2:1 by addition of saturated aqueous NaCl. The fractions containing the desired product were washed with water, and the organic layer was dried over Na_2SO_4 and evaporated under reduced pressure. The resulting dark purple solid was dissolved in a minimum amount of chloroform and reprecipitated by addition of hexane. The purple solid collected was washed with toluene and hexane and dried under vacuum to give **2** (21 mg, 55%): MALDI-TOF MS (dithranol) m/z 5935.32, calcd for $C_{294}H_{336}N_{30}O_{72}RuZn_6$ $(M - 2Cl^- + e^-)^+$ 5935.38; ESI-MS ($CHCl_3$) m/z 2967.5 $(M - 2Cl^-)^{2+}$; analytical GPC t_R = 10.9 min (as a single peak monitored from 254 to 750 nm by using a photodiode array detector) (conditions: column, TOSOH GMH_{HR}-M with guard column; eluent, chloroform:methanol = 98:2 v/v, 30 mM LiBr; flow rate, 0.8 mL/min); UV−vis ($CHCl_3$) λ_{max}/nm (ϵ) 627 (63700), 565 (81300), 426 (809500), 315 (130850).

UV−Vis and Fluorescence Titrations. All titration experiments were carried out in chloroform (containing 0.5% ethanol as a stabilizer) solution at 25 ± 0.5 °C. Typical procedures of the titration experiments are as follows. Chloroform (2 mL) was placed in a glass cell, and 10 μL of a 2 × 10^{-4} M **2** stock solution in chloroform was added to the cell to give a 1 × 10^{-6} M **2** solution. The glass cell was sealed with a septum cap to avoid evaporation. Then the UV−vis or fluorescence spectrum was recorded. A calculated amount of the amine stock solution in chloroform was added to the sample cell. The solution was stirred for 30−60 s, and the spectrum was recorded. Additional amounts of the amine stock solution were then added to the cell, and the spectrum was recorded after each addition. Total volumes of amine solution were less than 50 μL. Obtained data were analyzed according to ref 16.

Acknowledgment. This work was supported by the CREST (Core Research for Evolutional Science and Technology) program from JST (Japan Science and Technology Agency) and a Grant-in-Aid for Scientific Research on Priority Areas (No. 15036248), Reaction Control of Dynamic Complexes, from the Ministry of Education, Culture, Sports, Science and Technology, Japan (Monbu Kagakusho). A.S. acknowledges the financial assistance of a Grant-in-Aid for Young Scientists (B) in Grants-in-Aid for Scientific Research from Monbu Kagakusho and JSPS (Japan Society for the Promotion of Science).

Supporting Information Available: Preparation and synthetic procedures of **3**−**9**, MALDI-TOF mass spectra and gel permeation chromatographic analysis of **2**, UV−vis and fluorescence spectra of **1** and **2**, Hill plot analysis of **2** with *n*-$BuNH_2$, curve-fitting analysis and Job's plots of **2** with amines **3**−**6**, and H−H COSY, TOCSY, and HMQC spectra of 1:2 complex **2** with amine **3**.This material is available free of charge via the Internet at http://pubs.acs.org.

IC049645G

(24) Evans, I. P.; Spencer, A.; Wilkinson, G. *J. Chem. Soc., Dalton Trans.* **1973**, *2*, 204−209.